International Journal of Mass Spectrometry 298 (2010) 78–90

Contents lists available at ScienceDirect

International Journal of Mass Spectrometry

journal homepage: www.elsevier.com/locate/ijms

Metabolic profiling of human blood by high-resolution ion mobility mass spectrometry (IM-MS)

Prabha Dwivedi[a,*], Albert J. Schultz[b], Herbert H. Hill Jr[a,**]

[a] Department of Chemistry, Washington State University, Pullman, WA 99164, USA
[b] Ionwerks Inc., Houston, TX 77005, USA

ARTICLE INFO

Article history:
Received 29 September 2008
Received in revised form 3 February 2010
Accepted 10 February 2010
Available online 18 February 2010

Keywords:
Mobility-mass correlation curve (MMCC)
IMS
Isomer separation
Metabolomics
Blood metabolite
IM-MS

ABSTRACT

A high-resolution ion mobility time-of-flight mass spectrometer with electrospray ionization source (ESI-IM-MS) was evaluated as an analytical method for rapid analysis of complex biological samples such as human blood metabolome.

The hybrid instrument (IM-MS) provided an average ion mobility resolving power of ~90 and a mass resolution of ~1500 (at *m/z* 100). A few μL of whole blood was extracted with methanol, centrifuged and infused into the IM-MS via an electrospray ionization source. Upon IM-MS profiling of the human blood metabolome approximately 1100 metabolite ions were detected and 300 isomeric metabolites separated in short analyses time (30 min). Estimated concentration of the metabolites ranged from the low micromolar to the low nanomolar level. Various classes of metabolites (amino acids, organic acids, fatty acids, carbohydrates, purines and pyrimidines, etc.) were found to form characteristic mobility-mass correlation curves (MMCCs) that aided in metabolite identification. Peaks corresponding to various sterol derivatives, estrogen derivatives, phosphocholines, prostaglandins, and cholesterol derivatives detected in the blood extract were found to occupy characteristic two-dimensional IM-MS space. Low abundance metabolite peaks that can be lost in MS random noise were resolved from noise peaks by differentiation in mobility space. In addition, the peak capacity of MS increased sixfold by coupling IMS prior to MS analysis.

1. Introduction

1.1. Metabolomics

A parallel branch of biological science to proteomics, genomics, and transcriptomics that deals with the "omics" of metabolites and metabolism is called "metabolomics". Metabolites are small molecular weight compounds (<~1000 Da) that are employed as building blocks or produced as end products in various metabolic pathways and cellular regulatory processes in a biological system [1,2]. The entire collection of metabolites in a biological system, whether at the cellular, pathway or organism level, is known as a "metabolome". Levels of these metabolites in a metabolome are either dictated by the genome, proteome, and/or transcriptome of the biological system or imposed by environmental perturbations and results in changes in phenotype [3–5]. Thus metabolomics can be applied to map or identify the cause of alteration in phenotype and understand correlations between "omics" [6].

1.2. Blood analysis

Determination of metabolites present in blood samples provides insight into many human disease mechanisms and identifies biomarkers for disease diagnosis [7–10]. For example, metabolic profiling of amino acids and acylcarnitines is a powerful diagnostic tool in the diagnosis of inborn errors of metabolism (IEMs) such as phenylketonuria (PKU), medium-chain acyl-CoA dehydrogenase deficiency (MCAD); glutaric acidemia (GA), multiple carboxylase deficiency (MCD), isovaleric acidemia (IVA) and other inherent metabolic disorders (IMDs) [11,12]. Similarly, monitoring of various metabolic biomarkers present in blood is utilized for diagnosis for several diseases. Multiple sclerosis [13], HIV-1 [14], rotavirus gastroenteritis patients [15], influenza-associated encephalopathy [16], cystic fibrosis [17,18], congenital adrenal hyperplasia (CAH) [19], Antley-Bixler syndrome (ABS) and apparent pregnene hydroxylation deficiency (APHD) [20], Gaucher type 3 disease [21], cancer [22], Fabry's disease, glycolipid lipidosis [23], atherosclerosis [24], blood-circulation disorders [25], acute hepatitis [26], anemia and

* Corresponding author. Tel.: +1 509 335 7752; fax: +1 509 335 8867.
** Corresponding author. Tel.: +1 509 335 5648; fax: +1 509 335 8867.
E-mail addresses: pdwivedi@wsu.edu (P. Dwivedi), hhhill@wsu.edu (H.H. Jr).

1387-3806/$ – see front matter © 2010 Elsevier B.V. All rights reserved.
doi:10.1016/j.ijms.2010.02.007

glucose-6-phosphatase deficiency [27] are some of the diseases where metabolite(s) monitoring is applied for diagnostic/screening purposes.

1.3. Current analytical methods

Different metabolite analysis strategies can be applied to characterize a metabolome, such as (1) metabolite target analysis, (2) metabolite profiling, (3) metabolomics, (4) metabolic fingerprinting, (5) metabonomics, and (6) metabolic footprinting [10,28–30]. However, lack of efficient instrumental analytical techniques that can rapidly analyze complex biological samples and can provide sufficient visualization of the metabolome with diverse chemical and physical nature of metabolites require an array of analytical techniques for comprehensive analysis of a metabolome. Selection of the most suitable technique generally requires a compromise among speed, selectivity and sensitivity. Analytical separation methods such as gas chromatography [31–34], high-performance liquid chromatography [35–41], capillary electrophoresis [42–45], and ion-exchange chromatography [46] in tandem with mass spectrometry have been investigated for their application to metabolomics. Spectroscopic methods such as NMR have also been extensively explored for metabolomics studies [47–50]. Examples include application of NMR to assess effects of chemical, physical, and biological stressors on organisms [51,52]. Currently, NMR, GC, HPLC, and CE are extensively used in metabolic profiling and targeted metabolite analysis for disease diagnosis and treatment, detection and identification of biomarkers and drug synthesis and metabolism investigations [53–68].

In general, however, all of these methods require labor-intensive and time consuming sample preparation (extraction, derivatization, concentration, etc.) and are mostly suited for the analysis of a specific class of metabolites. Thus, there is a need for innovative approaches for measuring, monitoring and identifying the metabolome [69,70]. Techniques that would allow rapid and simultaneous determination of several classes of metabolites would not only increase sample throughput but also make profiling of metabolome possible under different stress conditions, and understanding relative variation of metabolites or metabolite classes under a specific stress condition. Such an analytical tool would enable identification of more biomarker(s) for the confirmation of diseases.

Ion mobility spectrometry coupled with mass spectrometry (IM-MS) is a rapid two-dimensional analytical tool and has been applied to various biological [71–73], pharmaceutical [74–78], environmental [79–82] and security related applications [83–85]. Feasibility of using IM-MS as a rapid analytical tool for metabolome profiling has been recently demonstrated where rapid separation and detection of hundreds of metabolites present in intracellular *E. coli* metabolome along with simultaneous separation of isomeric and isobaric metabolites was achieved [86]. This manuscript evaluates the potential of IM-MS for application to blood metabolome profiling.

2. Experimental

2.1. Chemicals and sample preparation

High-performance liquid chromatography grade solvents (methanol, water and acetic acid) were purchased from J. T. Baker (Phillips burgh, NJ). Blood samples were collected anonymously from the fingertips of the donor. The fingertips were first cleaned with sterilizing alcohol and then pierced with sterilized Glucose meter lancets (OneTouch UltraSoft) purchased from local departmental store (Rite Aid, Pullman, WA). Blood drops from fingertips were directly collected into methanol as extraction solvent. Approximately 50 μL of blood was added to 950 μL of methanol and acetic acid (1%) solution maintained at 40 °C over a heated water bath. The hot methanol–acetic acid–blood solution was kept in 40 °C water bath for 30 min and then centrifuged for 1 h at 1500 rpm. The supernatant was subjected to analysis by ESI-IM-MS without further sample preparation.

2.2. Instrumentation

The ESI-IM-MS instrument; schematic and picture shown in Fig. 1 was comprised of an electrospray ionization source, an ion mobility spectrometer operated at ambient pressure and a time-of-flight mass spectrometer.

2.2.1. Electrospray source

For electrospray ionization, samples were infused into a 15 cm long, 50 μm inner diameter silica capillary transfer line by a KD Scientific 210 syringe pump (New Hope, PA) at a flow rate of 4 μl/min. The capillary transfer line was connected to a 10 cm long, 50 μm inner diameter silica capillary through a stainless steel junction. A positive voltage of 15.12 kV was applied at the stainless steel junction to generate the electrospray. This 10 cm long capillary served as the electrospray needle and was centered ~0.5 cm from a target screen in the IMS.

2.2.2. Ion mobility spectrometer

A stacked-ring design ion mobility spectrometer used in this study was constructed at Washington State University as described in previous publications [87,88]. The APIMS tube was divided by a Bradbury-Nielsen ion gate into a 7.5 cm long desolvation region and a 17.3 cm long drift region. Both regions consisted of alternating alumina spacers and stainless steel rings with high temperature resistors connecting the stainless steel rings (500 kΩ resisters for the desolvation region, 1 MΩ resisters for the drift region). The ion gate was held at an electrical potential of 9934 V; with last ring of IMS at 285 V. Thus, the electric field was ~558 V/cm throughout the drift region. Using the Bradbury-Nielsen gate, ions were pulsed into the drift region with a pulse width of 0.2 ms. The temperature inside the IMS tube measured at the center of the desolvation region was 179 °C. Nitrogen was used as the drift gas at a flow rate of 1100 ml/min. During these studies the atmospheric pressure in Pullman, WA, was 703–705 Torr. The ESI source, the ion mobility spectrometer, and supporting electronics were designed and assembled at Washington State University, Pullman.

2.2.3. Pressure interface

To couple an ambient pressure IMS system to a low-pressure time-of-flight mass spectrometer, a interface was constructed at Ionwerks Inc., Houston, TX. The interface consisted of three ion lenses (nozzle, focusing, and skimmer) enclosed in a stainless steel chamber. The voltages applied on each element were: nozzle +74 V, focusing lens +62 V, skimmer +35 V. These setting provided optimum ion transmission through the interface with minimum ion fragmentation at the interface. However, any variation in the position of the IMS and/or voltage on the last IMS electrode would require optimization of the lens voltages. Ions exiting the IMS entered a differentially pumped chamber through a 250 μM aperture in the nozzle and entered the ion beam region of the MS through a 250 μM aperture in the skimmer.

2.2.4. Time-of-flight mass spectrometer

The time-of-flight mass spectrometer and supporting electronics were designed and constructed at Ionwerks Inc., Houston, TX. Ions entering through aperture were guided into the extraction region of the time-of-flight analyzer by a series of ion lenses. The ions were extracted orthogonally and accelerated to 4.5 kV

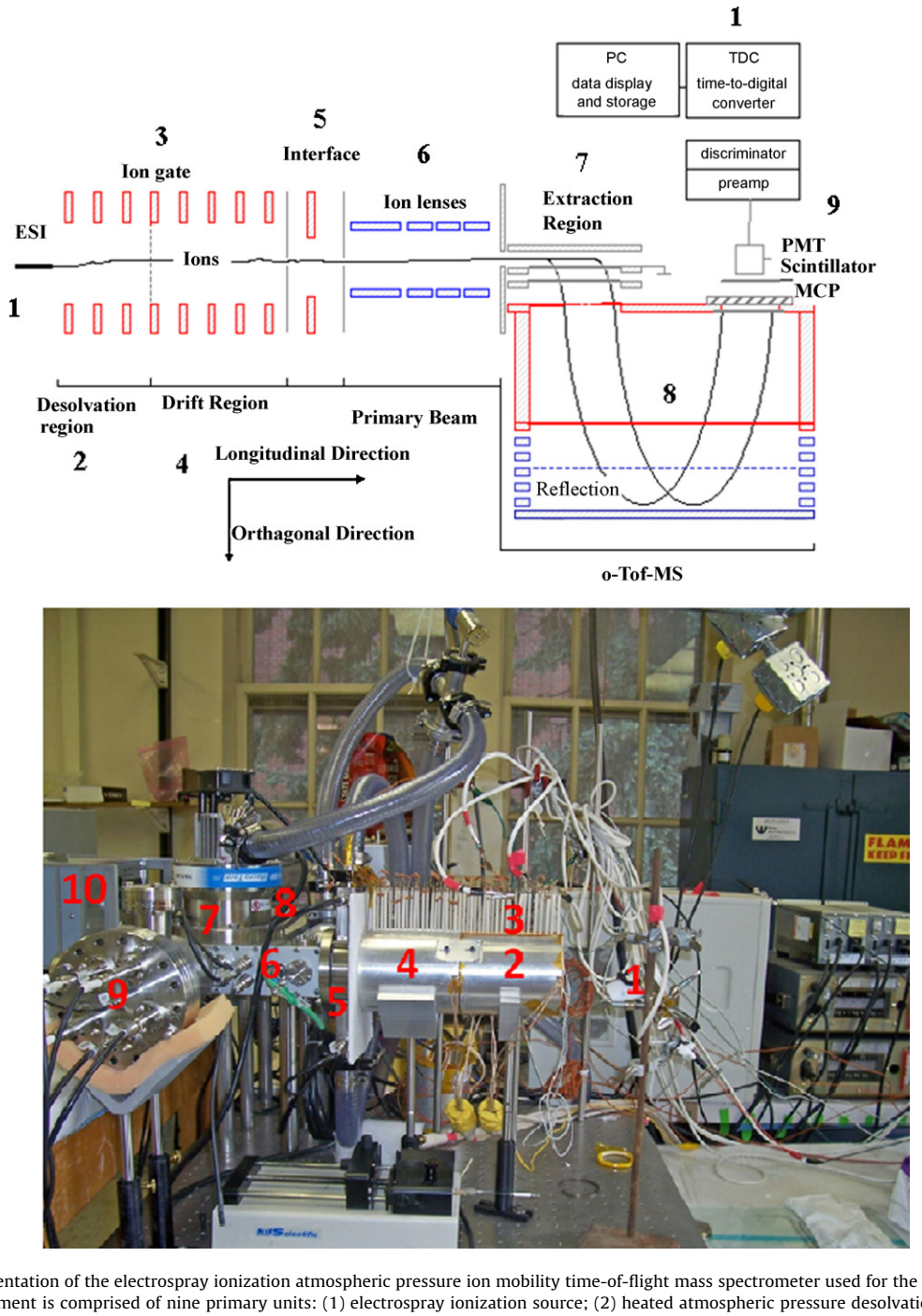

Fig. 1. Schematic representation of the electrospray ionization atmospheric pressure ion mobility time-of-flight mass spectrometer used for the analysis of human blood metabolome. This instrument is comprised of nine primary units: (1) electrospray ionization source; (2) heated atmospheric pressure desolvation region; (3) Bradbury-Nielsen ion gate; (4) counter-flow atmospheric pressure drift region; (5) differentially pumped interface; (6) ion guide with ion lenses; (7) extraction region; (8) reflectron time-of-flight mass analyzer, (9) bipolar MCP detector and (10) time-to-digital converter for data acquisition.

into the 40-cm-long reflectron drift tube and detected by a bipolar time-of-flight detector (Burle Electro-optics Inc., Sturbridge, MA). The detector signal was processed by a time-to-digital converter (TDCX4, Ionwerks Inc., Houston, TX). The ToF-MS operating voltages were as follows: $lens_1$ +24.6 V, $lens_2$ −22.1 V, deflector up −10.4 V, deflector down −14.0 V, $lens_3$ +108 V, reflector back 915.7 V, reflector grid −389.9 V, and bias 4.5 kV. The detector voltages were: photomultiplier tube −0.45 kV, scintillator +2.8 kV, and micro-channel plate (MCP) 0.9 kV.

2.2.5. Pressure considerations and data acquisition

Pressure in the interface (1.5 Torr), ion beam region (2×10^{-2} Torr) and reflectron region (1.4×10^{-6} Torr) was maintained using two Varian rough pumps (100 L/min DS102 and 600 L/min DS602) and two Varian turbo pumps (68 L/s-V70 and 250 L/s-V250). The IMS and the MS were scanned at 25 Hz and 25 kHz, respectively. Typical timing sequence and data acquisition has been described previously [89]. The two-dimensional IM-MS data was displayed as contour plots using IDL Virtual machine based software developed by Ionwerks Inc.

2.3. Basic IMS theory and calculations

Ion mobility spectrometry separates ions on the basis of the differences in their mobility K ($cm^2\ V^{-1}\ s^{-1}$) while the ions are drifting through a drift gas in a weak homogenous electric field gradient.

The mobility of an ion through the drift region of the ion mobility tube is given as the ratio of the average ion velocity $v_d = L/t_d$ to the applied electric field ($E = V/L$):

$$K = \frac{v_d}{E} = \frac{L^2}{t_d V} \quad (1)$$

where L is the length of the drift region in cm, t_d is the drift time in seconds (defined as the time an ion takes to travel through the drift region), and V is the voltage applied to the ion gate in volts. Experimental results are reported in terms of ion mobility reduced to standard temperature and pressure defined as: [K_o]

$$K_o = \frac{L^2}{Vt_d}\frac{273}{T}\frac{P}{760} \quad (2)$$

Separation of ionic species in IMS is achieved due to the differences in the collision cross-sections of the ions. Eq. (3) defines the average ion-neutral collision cross-section (Ω) measured in Å^2 in terms of measured mobility of the ion: [90]

$$\Omega = \left[\frac{3}{16N_A}\right]\left[\frac{2\pi}{\mu kT}\right]^{1/2}\left[\frac{ze}{K}\right] \quad (3)$$

where N_A is the number density of the drift gas in molecules per cm^3, μ [=$mM/(m+M)$] is the reduced mass in kilograms of an ion of mass m (g/mol) and the neutral drift gas of M (g/mol), k is Boltzmann's constant in J/K, z is the number of the charge(s) on the ion, e is the charge of one proton in coulombs and K is the mobility of the ion in cm^2 V^{-1} s^{-1}. Number density N_A is calculated as $N_A = (P/kT)$ where P is the atmospheric pressure in atmospheres, k is the Boltzmann's constant in L atm./K and T is the temperature in Kelvin.

3. Results and discussion

3.1. Resolving power, sensitivity, reproducibility, and dynamic range

The mass range of the time-of-flight mass spectrometer was calibrated through ESI-IM-MS analysis of 2,4-lutidine (m/z 107.2) and stachyose (m/z 666.6). Stachyose was detected as a sodium adduct

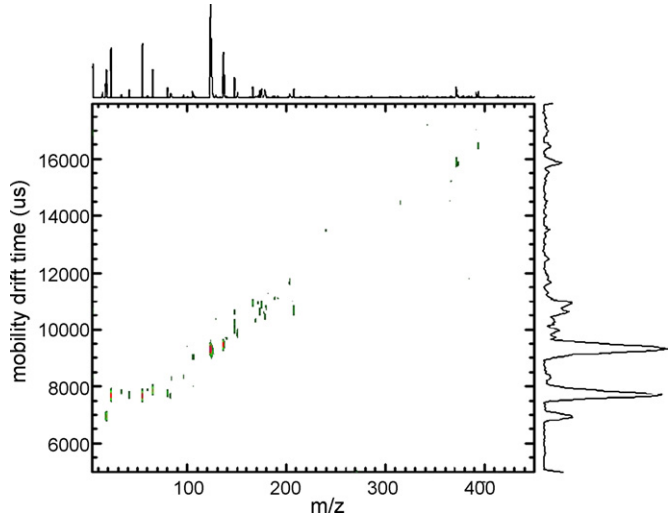

Fig. 2. 2D IM-MS spectrum of an equimolar (500 nM) metabolite mixture solution containing serine, nicotinamide, adenine, lysine, glutamine, ribose, phenylalanine, arginine, glucose, lactose, and maltose in 50:50 MeOH and H_2O with 1% acetic acid and 30 min data acquisition time is shown. All metabolites in the mixture were detected as one or more than one of the following adducts: $\{M(H_2O)_n+H\}^+$, $\{M(MeOH)_n+H\}^+$, $\{M(H_2O)_n+Na\}^+$ (Table 1).

Table 1
List of ions detected in an equimolar (500 nM) metabolite mixture solution.

Name	Mol. wt	Ion (m/z)	Reduced mobility (cm^2 V^{-1} s^{-1})	Ion identity
Water (H_2O)	18	19	2.19	$(M+H)^+$
Sodium	23	23	2.19	$(M)^+$
Methanol (MeOH)	32	33	2.15	$(M+H)^+$
Water	19	37	2.21	$(M_2+H)^+$
Sodium (Na)	23	41	2.19	$(M+H_2O)^+$
Water (H_2O)	18	55	2.19	$(M_3+H)^+$
Acetic acid (AcA)	60	61	2.13	$(M+H)^+$
Sodium	23	83	2.04	$(M+AcA)^+$
Serine	105	106	1.86	$(M+H)^+$
Nicotinamide	122	123	1.81	$(M+H)^+$
Adenine	135	136	1.78	$(M+H)^+$
Lysine	146	147	1.68	$(M+H)^+$
Glutamine	146	147	1.66	$(M+H)^+$
Ribose	150	151	1.58	$(M+H)^+$
Phenylalanine	165	166	1.54	$(M+H)^+$
Lysine	146	169	1.63	$(M+Na)^+$
Ribose	150	173	1.58	$(M+Na)^+$
Arginine	174	175	1.58	$(M+H)^+$
Glutamine	146	169	1.59	$(M+Na)^+$
Glucose	180	181	1.49	$(M+H)^+$
Phenylalanine	165	188	1.52	$(M+Na)^+$
Ribose	150	191	1.52	$(M+H_2O+Na)^+$
Glucose	180	203	1.45	$(M+Na)^+$
Lysine	146	207	1.53	$(M+AcA+H)^+$
Glutamine	146	207	1.58	$(M+AcA+H)^+$
Lactose	342	365	1.09	$(M+Na)^+$
Maltose	342	365	1.11	$(M+Na)^+$

Compound	Mass of ion	Reduced mobility		Ion identity
		Standard	Blood extract	
Serine	106	1.89	1.87	$(M+H)^+$
Threonine	120	1.82	1.79	$(M+H)^+$
Cysteine	122	1.80	1.78	$(M+H)^+$
Leucine	132	1.69	1.69	$(M+H)^+$
Aspargine	133	1.76	1.74	$(M+H)^+$
Lysine	147	1.70	1.69	$(M+H)^+$
Methionine	151	1.67	1.66	$(M+H)^+$
Histidine	156	1.67	1.65	$(M+H)^+$
Phenylalanine	166	1.56	1.55	$(M+H)^+$
Proline	116	1.85	1.82	$(M+H)^+$
Arginine	175	1.59	1.57	$(M+H)^+$
Tyrosine	182	1.49	1.47	$(M+H)^+$
Tryptophan	205	1.41	1.39	$(M+H)^+$
Ribose	173	1.58		$(M+Na)^+$
Glucose	203	1.46		$(M+Na)^+$
Maltose	365	1.1–1.25		$(M+Na)^+$

Identity of ions observed in an equimolar (500 nM) metabolite mixture solution containing serine, nicotinamide, adenine, lysine, glutamine, ribose, phenylalanine, arginine, glucose, lactose, and maltose in 50:50 MeOH and H_2O with 1% acetic acid.

$(M+Na)^+$ and 2,4-lutidine as a protonated monomer $(M+H)^+$. Average MS resolving power; measured using the equation $R = m/\Delta m$, where m is the mass of the peak and Δm is the full width at half maximum (FWHM), was 1500. Average resolving power of IMS defined as the ratio of the drift time of the ion to the peak width (in time) at half height ($R_p = t_d/w_h$) was measured to be 90. Reduced mobility value measured for 2,4-lutidine (m/z of 108) was $1.96 \pm .01$ cm^2 V^{-1} s^{-1} (literature value = 1.95). Average resolving power of first generation IM-MS constructed previously in our laboratory was 700 for the MS and 60 for the IMS [89].

To determine the reproducibility, detection limit, and dynamic range of IM-MS measurement, mixture solutions containing 11 metabolites (serine, nicotinamide, adenine, lysine, glutamine, ribose, phenylalanine, arginine, glucose, lactose, and maltose) each at 1 mM, 50 μM, and 500 nM concentrations prepared in 50:50 MeOH-H_2O with 1% acetic acid were analyzed by ESI-IM-MS. Interface Definition Language (IDL) files developed by IonWerks Inc. Houston, and executed using IDL virtual machine platform (IDL VM

6.2, ITT Visual Information Solutions, Boulder, CO) were used for data processing and visualization. In an unprocessed IM-MS spectrum the whole 2D IM-MS space is filled with noise and analyte signals as shown in Figure 2S, frame d (see supporting information). Adjustment of ion count threshold and averaging is employed to filter out noise peaks from the raw spectrum and the processed spectrum as shown in Fig. 4a is obtained. Due to variation in instrumental and chemical noise signals from one dataset to another the magnitude of threshold and averaging adapted to visualize a noise-free spectrum varies from one dataset to another. At present due to lack of an automatic noise recognition and removal tool "stare and compare strategy" was employed during noise removal. Theoretically, even one ion count above the noise level should be considered as an analyte signal. However, a simple curve (peak in this case) as defined by second degree polynomial equation ($y = ax^2 + bx + c$) will need three points, peaks with less than three ion counts were discarded. For reference, zoomed in IM-MS spectra showing IM-MS signals with 3, 5 and 45 ions counts for known analytes are also shown in frames a, b, and c in Figure 2S (supporting information). During presentation of some examples further in the text, the threshold was increased higher than needed to exclude noise signals just to reduce clutter of peaks in the IM-MS spectrum and or to minimize labor-intensive statistical data processing and metabolite identification. Low abundance metabolite peaks were thus not accounted for in the examples. An IM-MS spectrum for a 500 nM mixture solution of 11 metabolites is shown in Fig. 2. On the *x*-axis is shown the mass-to-charge ratio of the ions in Da and the *y*-axis represents the IMS drift time of ions in microseconds. All of the metabolites in the mixture were detected and identified as one or more than one of the following adduct ions $\{M(H_2O)_n+Na\}^+$, $\{M(H_2O)_n+H\}^+$, and $\{M(CH_3OH)_n+H\}^+$ (Table 1). Despite the fact that all metabolites were present in equimolar quantities in the mixture solution (500 nM), the number of ion counts for each metabolite peak ranged between 3 and ~100 counts. This variation in ion count with metabolite identity can be attributed to different ionization efficiencies of metabolites.

Various isomeric/isobaric ions (see Table 1; lysine and glutamine, lysine and ribose, lactose and maltose) were separated by IM-MS. Maximum standard deviations (triplicate measurements for 1 mM, 50 μM, and 500 nM mixture solutions) of 0.25 Da, 0.05 ms and 0.02 $cm^2\,V^{-1}\,s^{-1}$ in respectively *m*/*z*, drift time, and reduced mobility values were measured. Fig. 3 illustrates the reproducibility of the technique where Fig. 3a is an IM-MS contour plot of 1 μM solution of ribose analyzed in January 2006 and Fig. 3b–d

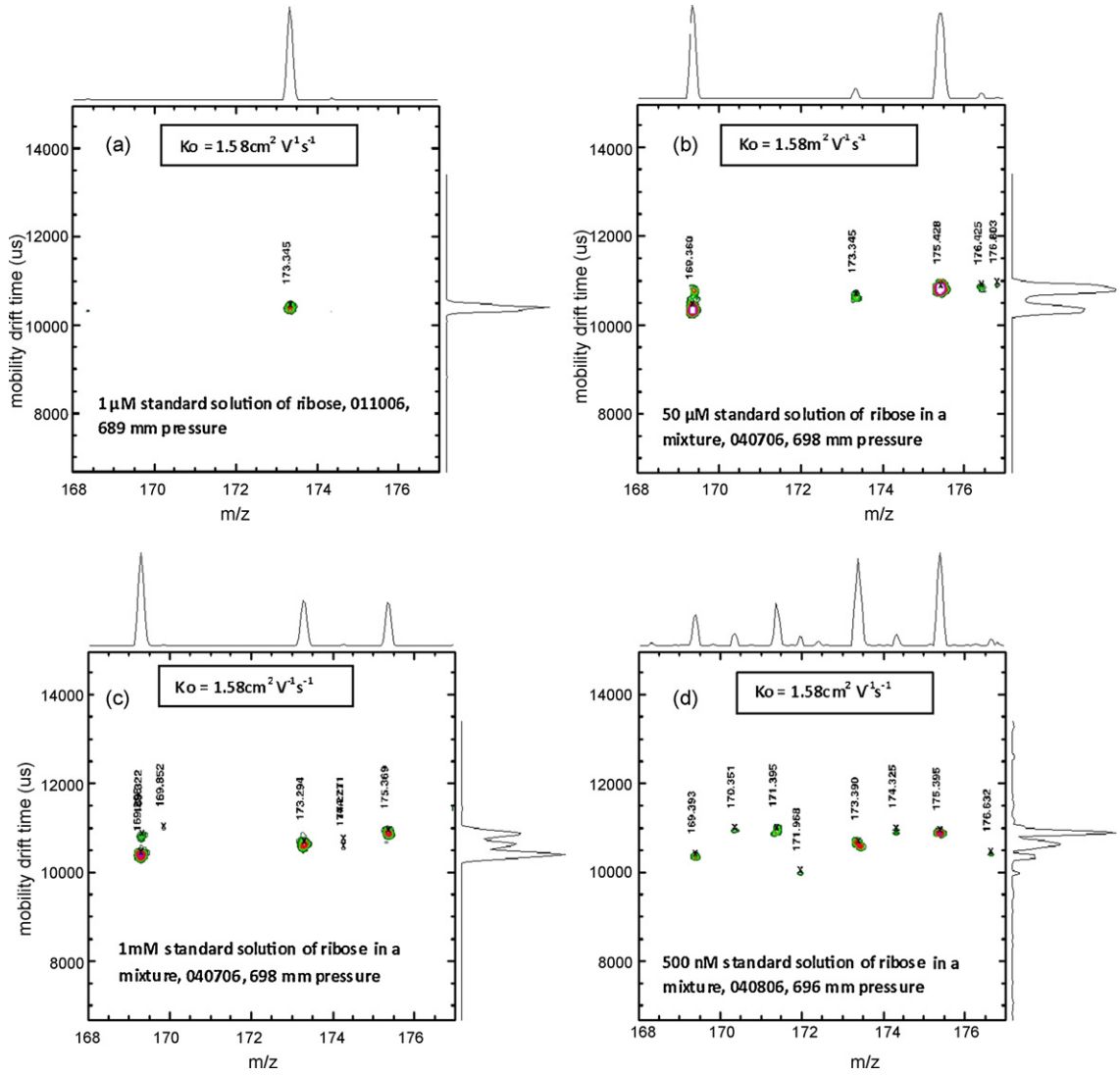

Fig. 3. Demonstration of reproducibility of reduced mobility value (K_o) of ribose as $(M+Na)^+$ ion measured for four different measurements at identical experimental conditions except for atmospheric pressure. Notice the reproducibility of K_o between measurements taken 3 months apart (between a and b/c/d). Figure also shows the effect of charge competition, ion suppression and preferential ionization of metabolites at different concentrations (1 mM to 500 nM).

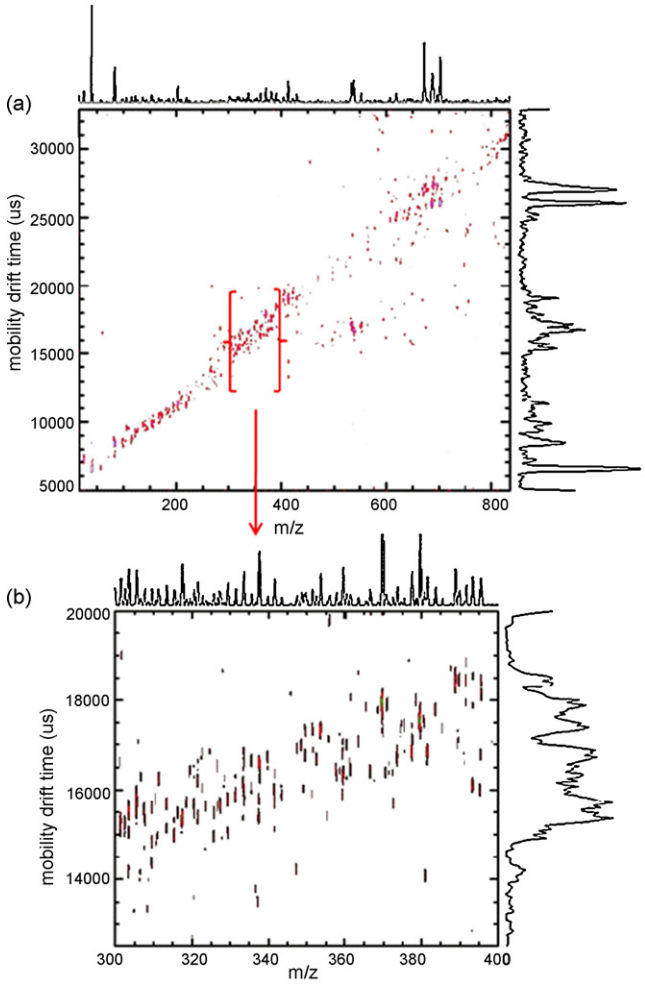

Fig. 4. (a) Two-dimensional spectrum of metabolic features measured in methanol extract of human blood. (b) A zoomed in section of the IM-MS spectrum in the *m*/*z* range of 300–400 Da illustrating the peaks detected in the region with 5 ion counts or more along with separation of isomers and isobars.

is 2D IM-MS plots of 1 mM, 50 μM, and 500 nM solutions equimolar metabolite mixture analyzed in April 2006, respectively. The reduced mobility value for ribose (*m*/*z* 173 Da) measured from mixtures in April 2006 (K_o = 1.58 $cm^2\ V^{-1}\ s^{-1}$) matched with the reduced mobility value of standard ribose solution measured in January 2006 (K_o = 1.58 $cm^2\ V^{-1}\ s^{-1}$).

Effects of charge competition and ion suppression were also evident upon analysis of equimolar mixtures of metabolites at varying concentrations. For example, peaks for lysine, adenine and nicotinamide were of highest intensity in the 500 nM mixture whereas in 1 mM and 50 μM metabolite mixture, the peak intensities for arginine and ribose were the strongest. Preferential ionization of an analyte was also evident. For example ribose as $(M+H_3O)^+$ ion at *m*/*z* 169 Da was observed at 5% intensity of the respective sodium adduct. 2D IM-MS plots for ribose detected with 5 and 45 ion counts as adducts of hydronium ion and sodium ion respectively are shown in frames b, and c in Figure 2S (supporting information).

Calibration curve for ribose as $(M+Na)^+$ at *m*/*z* value of 173 Da showed a linear relationship between peak intensity and concentration with a slope of 0.2 in the concentration range studied (1 mM to 500 nM). Linear but functional, not proportional, dependence of peak intensity on metabolite concentration was measured.

3.2. Blood analysis

3.2.1. IM-MS spectrum

ESI-IM-MS analysis of ESI solvent (water, methanol and acetic acid) produced ions that were identified as $\{M(H_2O)_n+H\}^+$, $\{M(H_2O)_n+Na\}^+$, $\{M(CH_3OH)_n+H\}^+$, $\{M(CH_3COOH)_n+H\}^+$, $\{M(H_2O)_n+K\}^+$, and $\{M(H_2O)_n+NH_4\}^+$ where M was either water, methanol, acetic acid. Fig. 4a illustrates a 2D IM-MS spectrum of the metabolite ions detected in hot methanol blood extract. On the *x*-axis is the mass-to-charge ratio of the ions in Da and the *y*-axis reports the IMS drift times of the ions in microseconds. The IM-MS spectra showed several high intensity metabolite and low intensity metabolite regions with ion counts for the peaks ranging between 3 and ~80. Extent of metabolite recovery in methanol, metabolite abundance in blood, number of isomers and isobars for each metabolite and/or variation in ionization efficiency of metabolites

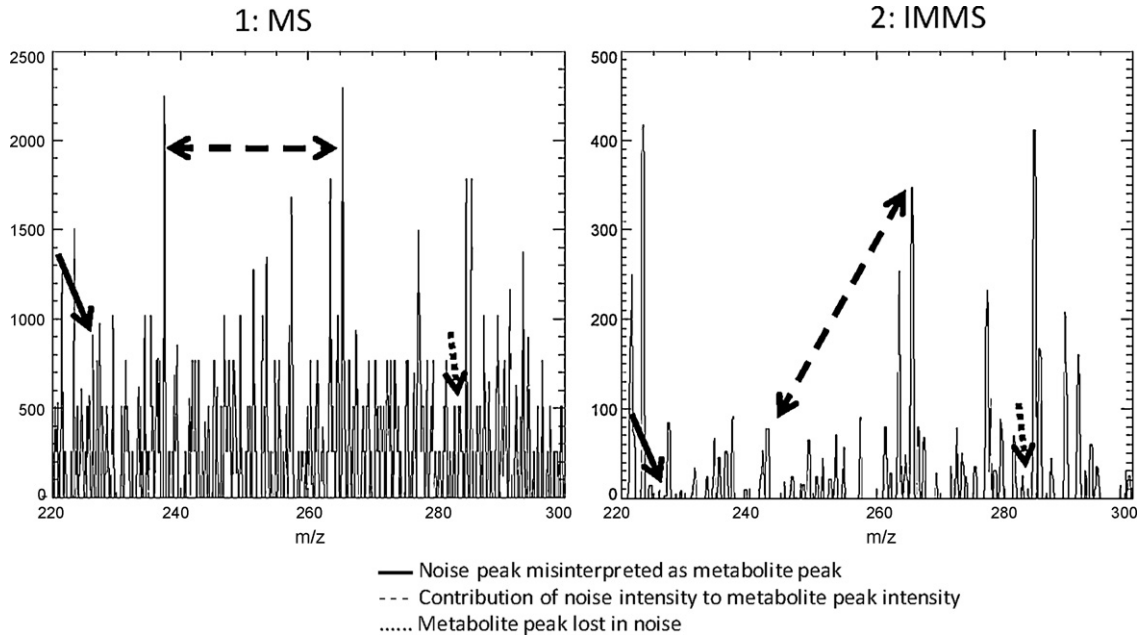

Fig. 5. One-dimensional mass spectrum (1) compared to one-dimensional mass spectrum with mobility differentiation (2). Three main features observed: (a) noise peak accounted as real peak (bold line), (b) contribution of random noise to peak intensity (dashed line), and (c) real peak lost in noise (dotted line).

contributes to variation in peak intensities of ions. Not all detected ions are visible in Fig. 4a due to relative ion-intensity differences. To visualize low abundance ions, the data file was processed in increments of 100 Da mass range as shown in Fig. 4b and signal threshold raised to exclude instrumental noise (dark counts) signals. A list of metabolites detected from the blood extract was generated with each peak characterized by its unique m/z value, drift time and intensity. Approximately ~1100 metabolite peaks with ion counts ≥3 and ~850 metabolite peaks with ion counts ≥5 were detected.

In an MS-only analysis, analyte peaks are characterized by their m/z values and their intensities. This is also true for the noise peaks. However in an IM-MS analysis the random noise peaks are not associated with unique mobility (drift time) values but instead are spread out in the mobility space in contrast to analyte peaks that are characterized by unique mobility values. Fig. 5 illustrates three different conditions when mobility measurements provide added advantages to MS analysis. Fig. 5(1) is a m/z spectrum where all detected peaks are shown and Fig. 5(2) is a m/z spectrum where only those peaks that also had unique mobility values are shown. On the x-axis is shown the mass-to-charge ratio of peaks and on the y-axis is shown the intensity of peaks detected. Comparison of intensities of peaks (shown with solid line arrows) in Fig. 5(1) and (2) illustrates an example where in the absence of mobility differentiation a noise peak can be considered to be an analyte peak. Similarly peaks shown with dotted line arrows illustrate an example when an analyte peak can be misinterpreted as noise peak. Contribution of noise peak intensity to the observed intensity of analyte peak is depicted through peaks shown with dashed line arrows in Fig. 5. Approximately fourfold decrease in peak intensity at m/z value of 237.4 relative to intensity of peak at m/z value of 265.4 was observed when contribution from noise peak intensity was considered.

3.2.2. Metabolite identification

3.2.2.1. Database search. Peaks detected in the blood extract were identified by comparing the m/z values of ions detected to the m/z values of metabolites listed in databases. The databases used were "METLIN-A metabolite mass spectral database", "LMSD: LIPID MAPS structure database" and "Golm Metabolome Database" [91–94]. The peaks were identified as metabolite ions as $\{M(H_2O)_n+H\}^+$, $\{M(H_2O)_n+Na\}^+$, $\{M(H_2O)_n(CH_3OH)+H\}^+$, $\{M(H_2O)_n(CH_3COOH)+H\}^+$, $\{M(H_2O)_n+K\}^+$, and/or $\{M(H_2O)_n+NH_4\}^+$ where M is a metabolite and n = 0–3. Peaks which were not identified could have been fragment ions of larger molecules or other adducts or clusters or unknown compounds. Similar to protein/peptide/metabolite identification via LC–MS methods that largely depend on spectral databases, development of IM-MS spectral databases becomes a necessity for the identification of metabolites present in biological samples. In addition, as has been reported for proteins and peptides [95–97], extension of two-dimensional IM-MS technique to higher order of dimensionality in separation (X^m–IM^n–MS^o, where "X" is an added dimension in separation) such as IM-MS/MS or LC–IM-MS/MS would allow confirmed identification of known metabolites and discovery of unknown metabolites. Various amino acids (arginine, tryptophan, etc.), carbohydrates (ribose, glucose, etc.), sugar phosphates (glucose-6-phosphate, fructose-6-phosphate), steroids (estrogen derivatives), nucleotides, nucleosides organic acids, bile acids (deoxycholic acid, lithocholic acid, etc.), acyl fatty acids (prostaglandin D2, E2, I2, etc.) glycerophospholipids (GPCho[17:0/14:1{9Z}], GPCho[16:0/18:1{9Z}], etc.), phospholipids are some of the classes of metabolites that were detected in the extract. Selected classes of metabolites detected as protonated ions are highlighted in Figure 6S and Table 2S (see supporting information) lists the metabolites detected with ≥5 ion counts along with their tentative identification. Identity of amino acids, pentose sugars and hexose sugars detected in blood extract were validated by comparing the m/z values and reduced mobility values of peaks detected in the blood extract to that measured for standard solutions using ESI-IM-MS. Following sections discuss selected classes of metabolites detected (validated and tentative).

3.2.2.2. Mobility-mass-correlation curves. Separation of various classes of compounds such as lipids and peptides based on characteristic mobility-mass-correlation curve (MMCC) formed in two-dimensional IM-MS space has been shown [98]. MMCC can provide a valuable tool in the identification of peaks detected in an IM-MS analysis of complex samples. Fig. 6 shows the different MMCCs observed for the various classes of metabolites detected in the blood extract by IM-MS.

Fig. 6A shows the 2D IM-MS plot in the m/z range of 50–250 and drift time range of 7–14 ms where peaks encircled correspond to the m/z values of protonated amino acids forming the MMCC. Identification of the peaks encircled was performed by comparing the reduced mobility values (K_o) measured using Eq. (2) for protonated ions of amino acids (50 μM standard solutions) to those detected in the blood sample. The insert in Fig. 6A shows the MMCC obtained by plotting the $1/K_o$ values measured for the standard solutions of amino acid peaks and the peaks identified as amino

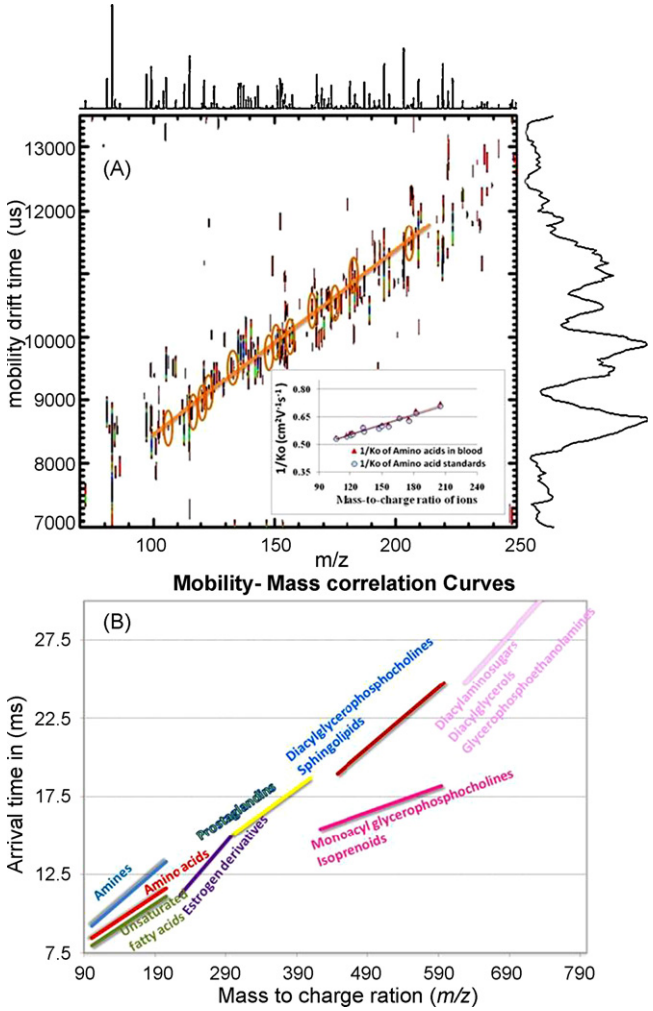

Fig. 6. (A) MMCC for amino acids detected in the blood extract. Peaks identified as amino acids in blood extract based on mass and reduced mobility data matched with that measured for standard solutions of amino acids. (B) MMCC for various classes of metabolites detected in the blood sample. Only protonated ions of metabolites constitute the MMCC (except for the sugars as sodium adducts).

acids in the blood extract against their respective m/z values (note the inverse relationship between drift time t_d and K_o in Eq. (2)). Distribution of amino acid peaks found in the blood along the MMCC similar to the MMCC obtained for the standard amino acid solutions supported the identification of the peaks as that of amino acids especially in cases where multiple peaks were detected at same m/z values. For example, at m/z 205.2 two isomeric metabolite peaks were observed at K_o values of 1.39 and 1.48 $cm^2\ V^{-1}\ s^{-1}$. The m/z values of the two peaks corresponded to m/z values of two endogenous metabolites, tryptophan (m/z 204.23) and oxalo-glutarate (m/z 204.14), detected as protonated ions. The peak at m/z 205.2 that had a K_o value of 1.39 $cm^2\ V^{-1}\ s^{-1}$ was identified as that of tryptophan since both the K_o value and the m/z value of the detected peak was within the standard deviation of that measured for a protonated ion of tryptophan standard ($1.41 \pm 0.02\ cm^2\ V^{-1}\ s^{-1}$). This peak also followed the MMCC for the amino acids which also supported the identification as tryptophan. Measured K_o values (blood and standard) and m/z values of detected amino acids are listed in Table 1. A maximum error of 2% was observed between the K_o values of amino acids detected in the blood extract and that of the standards. A deviation of 2% in K_o value is also generally observed in day-to-day IMS measurements.

Various isomers of monosaccharides were also detected and identification established. Sugars preferentially form sodium adducts upon ionization by ESI but are also detected in low abundance as adduct ions with proton, hydronium ion, protonated methanol, and potassium [99,100]. Pentose sugars were detected at m/z values of 151 (pentose + proton), 165 (methyl pentose + proton), 169 (pentose + hydronium ion), and 173 (pentose + sodium ion). Hexose sugars were detected at m/z values of 181 (hexose + proton), 195 (methylhexose + proton), 203 (hexose + sodium) and 219 (hexose + potassium). Similar to that of amino acids, isomeric sugars were distributed along a MMCC. Due to the isomeric nature of sugars, the sugar isomers were distributed in ~1 ms mobility space along the MMCC whereas the amino acids were confined in <0.5 ms mobility space. Identification of the detected peaks as sugar isomers were based on (1) comparison to K_o values of monosaccharides [99], (2) their respective m/z values, and (3) their position along the MMCC in the 2D IM-MS space.

Detection and confirmed identification of amino acids and sugars in the blood extract, demonstrate the strength of IM-MS for rapid analysis of complex biological samples to monitor targeted or comprehensive metabolites in the metabolome. Detection of free amino acids present in 50 μL of blood sample using IM-MS without any pre-concentration step demonstrates the potential of IM-MS to detect metabolites such as amino acids that are present in sub-micromolar concentration levels and usually require pre-concentration prior to analysis by chromatographic methods [101].

Fig. 6B shows some selected MMCCs formed by other classes of metabolites. Tentative identification of the metabolites forming the MMCCs was exclusively based on the m/z values of ions and only peaks corresponding to protonated ions $(M+H)^+$ of the metabolites were included.

Because drift times of ions increase with size of the ions, MMCCs also provide information on the structure of ions in addition to serving as a visual aide for the identification of metabolites in a complex spectrum. For example, in the 2D IM-MS space the amines occupied IM-MS space towards the longer drift times while the unsaturated fatty acids occupied the 2D space towards the shorter drift time relative to amino acid–carbohydrate MMCC (Figure 6S, A). This suggests that amines form less compact ions whereas the unsaturated fatty acids tend to form more compact ions upon ionization by ESI, relative to amino acids and monosaccharides. Similarly, in the m/z range of 380–600 Da (Figure 6S, B) sterols, diacylglycerophosphocholines, and sphingolipids were detected in the drift time range of 17–25 ms whereas the monoacylglycerophosphocholines and isoprenoids occupied the 2D space in the drift time range of 15–18 ms. Sterols and their derivatives such as stigmasterol, dihydrocholesterol, dihydroxy lanosterol, cholestane-triol have structures that constitute multiple 5 or 6 membered rings with a short hydrocarbon chain, that could prevent folding of the molecule upon ionization. Diacylglycerophosphocholines, with two hydrocarbon chains, formed less compact ions (drift time range of 17–25 ms) compared to the monoacylglycerophosphocholines and isoprenoids (drift time range of 15–18 ms). Review of the structures of sphingolipids and endogeneous blood isoprenoids, such as carotenoids and retinyl oleate [22,102], showed that the structures of sphingolipids are less favorable to folding due to two fatty acid tails and usually modified heads when compared to the structures of the isoprenoids that are in general single chain hydrocarbon derivatives. N-(hexadecanoyl)-sphinganine (ceramides), oleoyl-sphingosine, (3′-sulfo)Galβ-N-(acyl)-sphing-4-enine, and N-(9Z-octadecenoyl)-sphing-4-enine, diacylglycerophosphocholines, diacylglycerophosphoethanolamines are few of the sphingolipids and bisdehydro-β-carotene/tetradehydro-β-carotene (m/z 533), β-carotene (m/z 537), and 4-keto-γ-carotene/keto-γ-carotene (m/z 551) are few of the isoprenoids detected.

MMCC for protonated glycerophosphoethanolamines (for example at m/z 688, 698, 714, 736), and diacylglycerols (for example at m/z 605, 617, 618, 615, 642, 645, 660, 685, 701, 730) also show the effect of structural makeup of molecules on size of the ions. Note the high intensity peaks (Figure 6S, C) at m/z values of 672, 685, 688, and 701 Da corresponding to protonated glycosphingolipid [GlcCer(d18:1/14:0)], diacylglycerol [DG (19:0/22:5 (7Z,10Z,13Z,16Z,19Z)/0:0)], glycerophosphoethanolamine [GPEtn (16:1(9Z)/16:1(9Z))], and diacylglycerol [DG (20:1(11Z)/22:3(10Z,13Z,16Z)/0:0)]. Among these peaks, ions with higher drift times were that of glycosphingolipid at m/z 672 and glycerophosphoethanolamine at m/z 688 suggesting that these ions were relatively less dense than the diacylglycerols at m/z values of 685 and 701. This observation can be explained if the presence of comparatively larger head groups in the case of glycosphingolipid and glycerophosphoethanolamine compared to that of diacylglycerols resulted in the formation of relatively less compact ions due to hindered folding of the aliphatic chains.

MMCC for estrogen derivatives and prostaglandins (lipid biosynthesis/metabolism mediators) are also shown in Fig. 6B. Eicosanoids such as prostaglandins are biochemically synthesized from the arachidonic acid and are found in almost all tissues in the human body affecting many essential physiological functions such as contraction and relaxation of smooth muscle, the dilation and constriction of blood vessels, control of blood pressure, and modulation of inflammation [103]. Relative distribution of these metabolites serves as indicators of affects of regulatory mechanisms on specific metabolic pathways and thus ability to separate isomeric forms, detect, and monitor them simultaneously becomes important [104]. Examples of estrogen derivatives detected (circled in Figure 6S, D) include hydroxyestrapentanone (m/z 267), estrone (m/z 217), estradiol (m/z 273), hydroxyestradiol (m/z 289), andosterone (m/z 291) and methoxyestrone (m/z 301). Different prostaglandins were detected and are encircled in Figure 6S, E. Along with separation of various isomeric prostaglandins different forms of prostaglandins (PGA, PGB, PGC, PGD, PGE, PGF, PGG and their dimethyl, deoxy, glyceryl, keto, hydroxyl, ethanolamine, and phenyl derivatives) were detected. For example, three isomeric peaks, mass identified as that of PGA3, PGB3, and PGJ3, were separated in the mobility space at m/z value of 333.3 Da. Similarly, isomeric peaks at m/z value of 429.3 Da, possibly that of 2-Glyceryl-PGF2α and 1(3)-Glyceryl-PGF2α were mobility separated.

Figure 6S D also shows peaks at m/z values corresponding to that of octopine, arginosuccinic acid, deoxyinosine, guanosine, and xan-

thosine observed at m/z values of 265 ($M+H_3O^+$), 291 ($M+H^+$), 253 ($M+H^+$), 284 ($M+H^+$) and 285 ($M+H^+$), respectively. These endogeneous metabolites belong to various metabolic pathways such as arginine and proline metabolism pathway, alanine and aspartate metabolism pathway, and purine and caffeine metabolism pathway [94]. Isomeric pentose phosphates, hexose phosphates, hexose alcohol phosphates, hexose phosphoacids, and hexose N-acetyl amines as protonated and/or sodiated adducts are also encircled in Figure 6S, D. Peaks corresponding to the m/z values of protonated ions of purines and pyrimidines: adenine (m/z 137), guanine (m/z 152), thymine (m/z 127), cytosine (m/z 112), uracil (m/z 113), unsubstituted purine (m/z 121), xanthine (m/z 153), hypoxanthine (m/z 137) and uric acid (m/z 169) were detected.

Figure 6S F (IM-MS contour plot in the m/z range of 600–750 Da, see supporting information) illustrates another example where IMS when used as a pre-separation technique to MS measurements aids in the interpretation of peaks observed in a complex mass spectrum of biological samples. For example, isomeric pairs at m/z values of 619, 670, 696, and 712 Da (circled in Figure 6S, F). Interestingly, these isomers followed a MMCC suggesting that the ions observed at the above m/z values are structurally related [105–107]. Methylated heme (heme, M) has an m/z value of 618, thus the peaks at m/z values of 619, 670, 696 and 712 Da tentatively identified as (heme M+1)$^+$, (heme M+52)$^+$, (heme M+78)$^+$, (heme M+94)$^+$ ions, respectively. Structure of heme M (shown as insert in Figure 6S, F) shows that there are two potential sites for methylation (A and B) which may result in two isomeric structures.

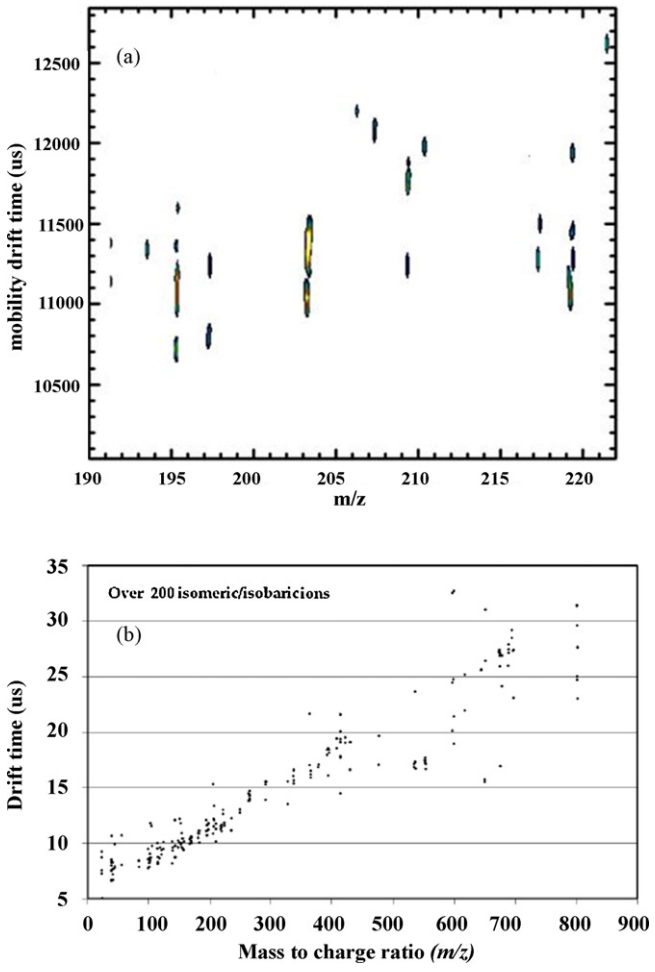

Fig. 7. (a) Enlarged section of Fig. 4a in the m/z range of 190–225 Da showing the separation of isomers/isobars by IMS. Four mobility separated peaks identified as potassium adducts of hexose sugars at m/z value of 219 Da along with four mobility separated peaks at m/z 195 Da and two mobility separated peaks each at m/z values of 191, 197, 209, 217, and 203 Da is illustrated. (b) Plot of drift time vs. m/z values of ions showing separation of over 200 isomeric/isobaric metabolite ions in blood extract detected by IM-MS with ≥10 ion counts.

3.2.3. Isomer separation

Diversity in lipid and carbohydrate structures and existence of each in various isomeric forms render lipid and carbohydrate profiling a very complicated and difficult task [108]. The most important contribution of ion mobility spectrometry in an IM-MS experiment is the separation of isomeric molecules simultaneous to detection by mass spectrometry. Fig. 7a is 2D IM-MS spectra in the m/z range of 190–225 Da, with peaks less than 10 ions counts excluded by raising the data processing threshold, demonstrating the separation of isomers by IMS. For example at an m/z value of 219 Da, four mobility separated peaks possibly potassium adducts of hexose sugars or sodium adducts of hexose sugar acids were detected. Similarly, four mobility separated peaks at m/z 195 Da and two mobility separated peaks each at m/z values of 191, 197, 209, 217, and 203 Da were detected. Isomeric peaks at m/z 203 were identified as sodium adducts of methylated glucose and mannose by comparing the reduced mobility values and m/z values obtained for the peaks detected in blood to that of standards of methylated glucose and mannose. Fig. 7b demonstrates the separation of over 200 isomeric/isobaric metabolites detected with ≥10 ion counts in blood extract by IM-MS analysis. On the x-axis is shown the mass-to-charge ratio of the ions in Da and the y-axis represents the drift time (IMS) of ions in microseconds. Two metabolite peaks with m/z values within m/z standard deviation of ±0.1 Da were considered isomers if their drift times were different by at least 0.2 ms. Isomeric ions corresponding to two glycerophosphoethanolamines GPEtn (18:1(9Z)/22:1(13Z); MW 799.6) and GPEtn (20:0/20:2(11Z,14Z); MW 799.6) detected at m/z 800.6 Da at drift times of 24.7 and 25.1 ms were separated with drift time difference of 0.4 ms. A drift time difference of 4.3 ms was observed between isomeric ions detected at m/z 801.7 and 801.8 Da corresponding to m/z values of protonated triacylglycerol, TG (16:1(9Z)/16:1(9Z)/16:1(9Z); m/z 800.7 Da) and that of dialkylglycerophosphocholine (m/z 800.6 Da) were observed at drift times of 27.6 and 23.1 ms. This experiment thus demonstrates that application of IM-MS to metabolomics would provide rapid detection of large number of metabolites present in complex biological matrix such as blood and simultaneous separation of isomeric species that cannot be easily differentiated by MS measurements alone.

3.2.4. Peak capacity of IM-MS

With tandem separation techniques such as IM-MS, CE–MS, LC–MS, maximum number of peaks that can fit in a two-dimensional space is defined as the peak capacity (φ) of the tandem method [109]. Thus peak capacity is a measure of the separation potential of the technique and depends on the resolution of the individual systems and difference in their separation mechanism (orthogonality). A 2D separation technique will have very high φ value if the fundamental separation mechanisms of individual high-resolution systems are completely different such as in LC–MS [110,111]. The peak capacity will also be defined by the complexity of the sample and the physical and chemical properties of the analytes in the sample. For example complex biological samples such as protein/peptide mixtures or metabolomes containing large number of analytes with varying chemical nature would provide larger peak capacities for the technique than that would be through the analysis of a mixture of analytes of a specific class. For example the peak capacity of LC–MS, where LC separations occur due to differences in partition coefficient of analyte ions between mobile phase and stationary phase and MS separation is based on their m/z ratios, is quite high due to completely different mechanism

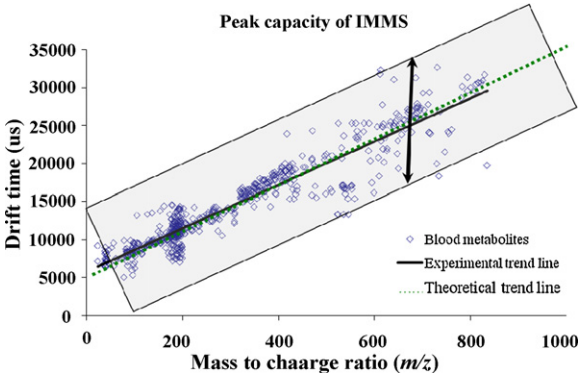

Fig. 8. Two-dimensional space (shaded area in the *X*–*Y* quadrant) occupied by metabolites that were detected in human blood extract by ESI-IM-MS (peak capacity) is illustrated. The theoretical MMCC (dotted line) is the centre line of the shaded area along which a constant drift time deviation should be observed. MMCC for the experimental data is depicted as bold line. The length of the 2D space is defined by the *m*/*z* range and width is defined by the maximum and minimum drift time deviation observed at a particular *m*/*z* value shown as double sided in the figure.

of separations involved in the individual analytical method [112]. With IM-MS as a tandem technique where separation occurs due to the differences in the Ω/z values (ion mobility) and *m*/*z* values (mass spectrometry), the plot of Ω/z versus *m*/*z* generally follow linear trend and thus exhibit smaller φ than LC–MS. With MS resolution of 400, IMS resolution of 60, and a maximum deviation of 11% in drift time, one- to fivefold increases in the peak capacity of the IM-MS method has been reported for a mixture of tryptic peptides (*m*/*z* range 500–2500). Though peak capacities of up to 10^7 can be achieved for LC–MS upon analysis of protein/peptide mixtures [113,114], number of metabolites detected in blood under single experimental condition has been reported to be between ~1000 and 3000 using LC–MS method [115–117]. However, even with limited orthogonality in separation, the high resolving power of IMS allowed separation of ~1100 metabolic features in a single experiment using the IM-MS method which is comparable to the number of metabolic features detected by LC–MS (~10^3). In addition, because ion mobility is a post-ionization gas phase separation method, temporal separation occurs in milliseconds resulting in very high peak production rate ($\varphi\,s^{-1}$). IM-MS as compared to LC–MS has at least three orders of magnitude greater $\varphi\,s^{-1}$ than LC–MS. An estimation of the peak capacity in IM-MS can be calculated as follows:

$$\Phi = \bar{R}_{IMS} \times \bar{R}_{MS} \times \text{fraction of orthogonality}$$

where $\bar{R}_{IMS}$ is the average resolving power of the ion mobility spectrometer, and $\bar{R}_{IMS}$ is the average resolution of the mass spectrometer in an *m*/*z* range. For example, in the mass range of 23–830 Da for the metabolites detected the minimum and maximum deviation in drift time along a vertical plane parallel to the *y*-axis defines the fraction of orthogonality as shown by double sided arrows in Fig. 8. The theoretical MMCC shown as dotted line in the figure is the centre line of the shaded area along which a constant drift time deviation should be observed whereas the MMCC obtained for the experimental data is depicted as bold line in Fig. 8. The length of the 2D space is defined by the *m*/*z* range and double sided arrow defines the drift time spread in the given *m*/*z* range. With a drift time spread of ~14.3 ms the total % deviation measures to be ~28% [14.3/(18.37/2 + 32.66/2)] of the total 2D space (Fig. 8, shaded space in the *X*–*Y* quadrant). This gives an average deviation in drift time of ±14% along the theoretical trend. With average IMS resolving power of 90, average MS resolution of 1500, and ±14% deviation, the estimated peak capacity for the instrument was ~18,900. With MS resolution of 1500, peak width at *m*/*z* 404 is 0.27 Da (for the *m*/*z* range of 23–830 Da the average *m*/*z* value is equal to 404 Da) the estimated peak capacity of MS alone was 2989. By using IMS in tandem with MS, sixfold increase in the peak capacity was observed (~19,000) compared to peak capacity of the MS as a standalone method of separation (~3000).

4. Conclusions

The high-resolution ion mobility mass spectrometer used in this study provided an average IMS resolving power of ~90 and MS resolution of ~1500. Reproducible reduced mobility values for metabolites in millimolar to nanomolar concentration range can be achieved. Without any pre-concentration, over 1100 metabolites can be detected in methanol extracts of 50 μL of blood samples. Along with the detection of metabolites in the blood extract, simultaneous separation of over 300 isomeric/isobaric metabolites can also be accomplished. Various classes of metabolites including amino acids, carbohydrates, endogenous amines, purines and pyrimidines, organic acids, sterols, estrogens, prostaglandins, phosphocholines, mono- and diacylglycerophosphoethanolamines, mono- and diacylglycerols, sphingolipids, isoprenoids and various metabolic intermediates can be concurrently detected and separated in a 2D IM-MS analysis. Peak capacity of mass spectrometers can be increased by a factor of six by coupling of IMS as a pre-separation technique prior to MS analysis which can be further increased by increasing the separation power of IMS and MS.

An important advantage of IM-MS is the separation of similar classes of metabolites along a unique MMC lines that can be used to complement and facilitate identification of metabolites detected by MS. Two-dimensional IM-MS analysis facilitates separation of random noise peaks from low intensity metabolite peaks through differentiation in mobility space and thus make possible detection of low abundance metabolites.

When compared to LC–MS when applied to blood metabolite detection, IM-MS even with limited orthogonality in separation, demonstrated detection of comparable number of metabolic features in the blood metabolome due to high resolving power of the IMS. Ion mobility mass spectrometry with its ability to rapidly provide high-resolution comprehensive complex sample analyses and its compatibility with various analytical methods such as chromatography appears to be a promising new analytical technique for the assessment of metabolomes. Further improvement in IM-MS separation power and ion transmission efficiency would significantly enhance the potential of IM-MS as applied to metabolomics studies. Development of IM-MS spectral databases and multidimensional instrumentation and data processing software would allow rapid metabolome analysis and interpretation.

Acknowledgements

This work was supported in part by a grant from National Institute of Health-Road Map Grant #R21-DK070274. We also would like to thank Mr. Roger H. Crawford at Washington State University in Pullman, WA and Drs. Agnes Tempez, and Thomas F. Egan at Ionwerks Inc. in Houston, TX for their help throughout this project.

Appendix A. Supplementary data

Supplementary data associated with this article can be found, in the online version, at doi:10.1016/j.ijms.2010.02.007.

References

[1] L.N. David, M.C. Michael, Lehninger Principles of Biochemistry, fourth edition, W. H. Freeman, 2004.

[2] G. Michal, in: G. Michal (Ed.), Biochemical Pathways: An Atlas of Biochemistry and Molecular Biology, John Wiley & Sons, New York, 1999.
[3] R. Goodacre, Metabolomics—the way forward, Metabolomics 1 (1) (2005) 1–2.
[4] R. Goodacre, S. Vaidyanathan, W.B. Dunn, G.G. Harrigan, D.B. Kell, Metabolomics by numbers: acquiring and understanding global metabolite data, Trends in Biotechnology 22 (5) (2004) 245–252.
[5] G.H. Thomas, Metabolomics breaks the silence, Trends in Microbiology 9 (4) (2001) 158–1158.
[6] E.C. Horning, M.G. Horning, Metabolic profiles: gas-phase methods for analysis of metabolites, Clinical Chemistry 17 (8) (1971) 802–809.
[7] T. Dunckley, K.D. Coon, D.A. Stephan, Discovery and development of biomarkers of neurological disease, Drug Discovery Today 10 (5) (2005) 326–334.
[8] D.A. Fell, Beyond genomics, Trends in Genetics 17 (12) (2001) 680–682.
[9] A.R. Fernie, R.N. Trethewey, A.J. Krotzky, L. Willmitzer, Innovation—metabolite profiling: from diagnostics to systems biology, Nature Reviews Molecular Cell Biology 5 (9) (2004) 763–769.
[10] O. Fiehn, Metabolomics—the link between genotypes and phenotypes, Plant Molecular Biology 48 (1–2) (2002) 155–171.
[11] N. Kodo, D.S. Millington, D.L. Norwood, C.R. Roe, Quantitative assay of free and total carnitine using tandem mass spectrometry, Clinica Chimica Acta 186 (3) (1990) 383–390.
[12] M.S. Rashed, M.P. Bucknall, D. Little, A. Awad, M. Jacob, M. Alamoudi, M. Alwattar, P.T. Ozand, Screening blood spots for inborn errors of metabolism by electrospray tandem mass spectrometry with a microplate batch process and a computer algorithm for automated flagging of abnormal profiles, Clinical Chemistry (Washington, D.C.) 43 (7) (1997) 1129–1141.
[13] G. Giovannoni, S.J.R. Heales, N.C. Silver, J. O'Riordan, R.F. Miller, J.M. Land, J.B. Clark, E.J. Thompson, Raised serum nitrate and nitrite levels in patients with multiple sclerosis, Journal of the Neurological Sciences 145 (1) (1997) 77–81.
[14] R. Zangerle, D. Fuchs, G. Reibnegger, G. Werner-Felmayer, H. Gallati, H. Wachter, E.R. Werner, Serum nitrite plus nitrate in infection with human immunodeficiency virus type-1, Immunobiology 193 (1) (1995) 59–70.
[15] H. Kawashima, Y. Inage, M. Ogihara, Y. Kashiwagi, K. Takekuma, A. Hoshika, T. Mori, Y. Watanabe, Serum and cerebrospinal fluid nitrite/nitrate levels in patients with rotavirus gastroenteritis induced convulsion, Life Sciences 74 (11) (2004) 1397–1405.
[16] H. Kawashima, Y. Watanabe, T. Ichiyama, M. Mizuguchi, N. Yamada, Y. Kashiwagi, K. Takekuma, A. Hoshika, T. Mori, High concentration of serum nitrite/nitrate obtained from patients with influenza-associated encephalopathy, Pediatrics International 44 (6) (2002) 705–707.
[17] P.K. Zarzycki, K.M. Kulhanek, R. Smith, V.L. Clifton, Determination of steroids in human plasma using temperature-dependent inclusion chromatography for metabolomic investigations, Journal of Chromatography A 1104 (1–2) (2006) 203–208.
[18] V. Figueroa, C. Milla, E.J. Parks, S.J. Schwarzenberg, A. Moran, Abnormal lipid concentrations in cystic fibrosis, American Journal of Clinical Nutrition 75 (6) (2002) 1005–1011.
[19] M.P. Caulfield, T. Lynn, M.E. Gottschalk, K.L. Jones, N.F. Taylor, E.M. Malunowicz, C.H.L. Shackleton, R.E. Reitz, D.A. Fisher, The diagnosis of congenital adrenal hyperplasia in the newborn by gas chromatography/mass spectrometry analysis of random urine specimens, The Journal of Clinical Endocrinology and Metabolism 87 (8) (2002) 3682–3690.
[20] C. Shackleton, Biochemical diagnosis of Antley-Bixler syndrome by steroid analysis, American Journal of Medical Genetics Part A 128A (3) (2004) 223–231.
[21] R. Gornati, B. Bembi, X. Tong, R. Boscolo, B. Bruno, Total glycolipid and glucosylceramide content in serum and urine of patients with Gaucher's disease type 3 before and after enzyme replacement therapy, Clinica Chimica Acta 271 (2) (1998) 151–161.
[22] X. Zhang, L. Kiechle Frederick, Review: glycosphingolipids in health and disease, Annals of Clinical and Laboratory Science 34 (1) (2004) 3–13.
[23] D.E. Vance, W. Krivit, C.C. Sweeley, Concentrations of glycosyl ceramides in plasma and red cells in Fabry's disease, a glycolipid lipidosis, Journal of Lipid Research 10 (2) (1969) 188–192.
[24] A.R. Tall, X.C. Jiang, Detection and Treatment of Atherosclerosis based on Plasma Sphingomyelin Concentration. Application, Trustees of Columbia University in the City of New York, USA, WO, 2001, 76 pp.
[25] S.A. Mirzoyan, E.E. Mkheyan, E.S. Sekoyan, E.K. Grigoryan, G.O. Bakunts, Blood glycolipids in patients with brain blood-circulation disorders, Zhurnal Nevropatologii i Psikhiatrii imeni S. S. Korsakova 78 (9) (1978) 1317–1322.
[26] W. Atzpodien, G. Huewels, G.J. Kremer, E. Schnellbacher, Study of plasma glycosphingolipids in acute hepatitis, Verhandlungen der Deutschen Gesellschaft fuer Innere Medizin 82 (1) (1976) 429–431.
[27] M.J. Markuszewski, M. Szczykowska, D. Siluk, R. Kaliszan, Human red blood cells targeted metabolome analysis of glycolysis cycle metabolites by capillary electrophoresis using an indirect photometric detection method, Journal of Pharmaceutical and Biomedical Analysis 39 (3–4) (2005) 636–642.
[28] K. Dettmer, B.D. Hammock, Metabolomics—a new exciting field within the "omics" sciences, Environmental Health Perspectives 112 (7) (2004) A396–A397.
[29] W.B. Dunn, D.I. Ellis, Metabolomics: current analytical platforms and methodologies, Trends in Analytical Chemistry 24 (4) (2005) 285–294.
[30] O. Fiehn, Combining genomics, metabolome analysis, and biochemical modelling to understand metabolic networks, Comparative and Functional Genomics 2 (3) (2001) 155–168.
[31] A. Jiye, J. Trygg, J. Gullberg, A.I. Johansson, P. Jonsson, H. Antti, S.L. Marklund, T. Moritz, Extraction and GC/MS analysis of the human blood plasma metabolome, Analytical Chemistry 77 (24) (2005) 8086–8094.
[32] J.L. Hope, B.J. Prazen, E.J. Nilsson, M.E. Lidstrom, R.E. Synovec, Comprehensive two-dimensional gas chromatography with time-of-flight mass spectrometry detection: analysis of amino acid and organic acid trimethylsilyl derivatives, with application to the analysis of metabolites in rye grass samples, Talanta 65 (2) (2005) 380–388.
[33] J.E. Katz, D.S. Dumlao, S. Clarke, J. Hau, A new technique (COMSPARI) to facilitate the identification of minor compounds in complex mixtures by GC/MS and LC/MS: tools for the visualization of matched datasets, Journal of the American Society for Mass Spectrometry 15 (4) (2004) 580–584.
[34] J. Taylor, D. King Ross, T. Altmann, O. Fiehn, Application of metabolomics to plant genotype discrimination using statistics and machine learning, Bioinformatics (Oxford, England) 18 (Suppl. 2) (2002) S241–S248.
[35] P.H. Gamache, D.F. Meyer, M.C. Granger, I.N. Acworth, Metabolomic applications of electrochemistry/mass spectrometry, Journal of the American Society for Mass Spectrometry 15 (12) (2004) 1717–1726.
[36] W. Lu, E. Kimball, J.D. Rabinowitz, A high-performance liquid chromatography–tandem mass spectrometry method for quantitation of nitrogen-containing intracellular metabolites, Journal of the American Society for Mass Spectrometry 17 (1) (2006) 37–50.
[37] H. Pham-Tuan, L. Kaskavelis, A. Daykin Clare, H.-G. Janssen, Method development in high-performance liquid chromatography for high-throughput profiling and metabonomic studies of biofluid samples, Journal of Chromatography B, Analytical Technologies in the Biomedical and Life Sciences 789 (2) (2003) 283–301.
[38] K.E. Vigneau-Callahan, A.I. Shestopalov, P.E. Milbury, W.R. Matson, B.S. Kristal, Characterization of diet-dependent metabolic serotypes: analytical and biological variability issues in rats, Journal of Nutrition 131 (3) (2001) 924S–932S.
[39] S. Wagner, K. Scholz, M. Donegan, L. Burton, J. Wingate, W. Voelkel, Metabonomics and biomarker discovery: LC–MS metabolic profiling and constant neutral loss scanning combined with multivariate data analysis for mercapturic acid analysis, Analytical Chemistry 78 (4) (2006) 1296–1305.
[40] D. Wilson Ian, R. Plumb, J. Granger, H. Major, R. Williams, M. Lenz Eva, HPLC–MS-based methods for the study of metabonomics, Journal of Chromatography B, Analytical Technologies in the Biomedical and Life Sciences 817 (1) (2005) 67–76.
[41] J. Yang, X. Zhao, X. Liu, C. Wang, P. Gao, J. Wang, L. Li, J. Gu, S. Yang, G. Xu, High performance liquid chromatography–mass spectrometry for metabonomics: potential biomarkers for acute deterioration of liver function in chronic hepatitis B, Journal of Proteome Research 5 (3) (2006) 554–561.
[42] Anon., Research profile; CE/MS for quantitative metabolome analysis, Journal of Proteome Research 2 (5) (2003) 463.
[43] S. Sato, T. Soga, T. Nishioka, M. Tomita, Simultaneous determination of the main metabolites in rice leaves using capillary electrophoresis mass spectrometry and capillary electrophoresis diode array detection, Plant Journal 40 (1) (2004) 151–163.
[44] T. Soga, Y. Ohashi, Y. Ueno, H. Naraoka, M. Tomita, T. Nishioka, Quantitative metabolome analysis using capillary electrophoresis mass spectrometry, Journal of Proteome Research 2 (5) (2003) 488–494.
[45] B.C.V. Suresh, E.J. Song, S.M.E. Babar, M.H. Wi, Y.S. Yoo, Capillary electrophoresis at the omics level: towards systems biology, Electrophoresis 27 (1) (2006) 97–110.
[46] X. Chen, L. Kong, X. Su, C. Pan, M. Ye, H. Zou, Integration of ion-exchange chromatography fractionation with reversed-phase liquid chromatography–atmospheric pressure chemical ionization mass spectrometer and matrix-assisted laser desorption/ionization time-of-flight mass spectrometry for isolation and identification of compounds in Psoralea corylifolia, Journal of Chromatography A 1089 (1–2) (2005) 87–100.
[47] E.M. Lenz, J. Bright, I.D. Wilson, S.R. Morgan, A.F.P. Nash, A ^{1}H NMR-based metabonomic study of urine and plasma samples obtained from healthy human subjects, Journal of Pharmaceutical and Biomedical Analysis 33 (5) (2003) 1103–1115.
[48] R. Bhalla, K. Narasimhan, S. Swarup, Metabolomics and its role in understanding cellular responses in plants, Plant Cell Reports 24 (10) (2005) 562–571.
[49] A.W. Nicholls, E. Holmes, J.C. Lindon, J.P. Shockcor, R.D. Farrant, J.N. Haselden, S.J. Damment, C.J. Waterfield, J.K. Nicholson, Metabonomic investigations into hydrazine toxicity in the rat, Chemical Research in Toxicology 14 (8) (2001) 975–987.
[50] E. Holmes, A.W. Nicholls, J.C. Lindon, S.C. Connor, J.C. Connelly, J.N. Haselden, S.J. Damment, M. Spraul, P. Neidig, J.K. Nicholson, Chemometric models for toxicity classification based on NMR spectra of biofluids, Chemical Research in Toxicology 13 (6) (2000) 471–478.
[51] H. Wu, X. Zhang, P. Liao, Z. Li, W. Li, X. Li, Y. Wu, F. Pei, NMR spectroscopic-based metabonomic investigation on the acute biochemical effects induced by $Ce(NO_3)_3$ in rats, Journal of Inorganic Biochemistry 99 (11) (2005) 2151–2160.
[52] M.R. Viant, E.S. Rosenblum, R.S. Tieerdema, NMR-based metabolomics: a powerful approach for characterizing the effects of environmental stressors on organism health, Environmental Science & Technology 37 (21) (2003) 4982–4989.
[53] G. Pendyala, E.J. Want, W. Webb, G. Siuzdak, H.S. Fox, Biomarkers for neuroAIDS: the widening scope of metabolomics, Journal of Neuroimmune Pharmacology 2 (1) (2007) 72–80.

[54] W.B. Dunn, Current trends and future requirements for the mass spectrometric investigation of microbial, mammalian and plant metabolomes, Physical Biology 5 (1) (2008) 11001.
[55] J.P. Godin, L.B. Fay, G. Hopfgartner, Liquid chromatography combined with mass spectrometry for ^{13}C isotopic analysis in life science research, Mass Spectrometry Reviews 26 (6) (2007) 751–774.
[56] T.O. Metz, Q. Zhang, J.S. Page, Y. Shen, S.J. Callister, J.M. Jacobs, R.D. Smith, The future of liquid chromatography–mass spectrometry (LC–MS) in metabolic profiling and metabolomic studies for biomarker discovery, Biomarkers in Medicine 1 (1) (2007) 159–185.
[57] R.F. Witkamp, Genomics and systems biology—how relevant are the developments to veterinary pharmacology, toxicology and therapeutics? Journal of Veterinary Pharmacology and Therapeutics 28 (3) (2005) 235–245.
[58] G.J. Ad de Jong, Foreword: new developments in CE, CIEF and CE for metabolomics, Journal of Chromatography A 1204 (2) (2008) 129.
[59] C. Barbas, M. Vallejo, A. Garcia, D. Barlow, M. Hanna-Brown, Capillary electrophoresis as a metabolomic tool in antioxidant therapy studies, Journal of Pharmaceutical and Biomedical Analysis 47 (2) (2008) 388–398.
[60] M.R. Monton, T. Soga, Metabolome analysis by capillary electrophoresis–mass spectrometry, Journal of Chromatography A 1168 (1–2) (2007) 237–246 (discussion 236).
[61] R. Ramautar, G.W. Somsen, G.J. de Jong, CE–MS in metabolomics, Electrophoresis 30 (1) (2009) 276–291.
[62] T. Soga, Capillary electrophoresis–mass spectrometry for metabolomics, Methods in Molecular Biology 358 (2007) 129–137.
[63] F. van der Kooy, F. Maltese, Y.H. Choi, H.K. Kim, R. Verpoorte, Quality control of herbal material and phytopharmaceuticals with MS and NMR based metabolic fingerprinting, Planta Medica 75 (7) (2009) 763–775.
[64] E.F. Queiroz, J.L. Wolfender, K. Hostettmann, Modern approaches in the search for new lead antiparasitic compounds from higher plants, Current Drug Targets 10 (3) (2009) 202–211.
[65] R. Powers, NMR metabolomics and drug discovery, Magnetic Resonance in Chemistry 47 (S1) (2009) S2–S11.
[66] S. Vangala, A. Tonelli, Biomarkers, metabonomics, and drug development: can inborn errors of metabolism help in understanding drug toxicity? The AAPS Journal 9 (3) (2007) E284–E297.
[67] H. Orhan, Analyses of representative biomarkers of exposure and effect by chromatographic, mass spectrometric, and nuclear magnetic resonance techniques: method development and application in life sciences, Journal of Separation Science 30 (2) (2007) 149–174.
[68] D.S. Sem, M. Pellecchia, NMR in the acceleration of drug discovery, Current Opinion in Drug Discovery & Development 4 (4) (2001) 479–492.
[69] C.D. DeAngelis, E.A. Zerhouni, N.I.H. Director Elias, A. Zerhouni, MD, reflects on agency's challenges, priorities, Journal of the American Medical Association 289 (12) (2003) 1492–1493.
[70] E. Zerhouni, The NIH roadmap, Science 302 (5642) (2003).
[71] S.J. Valentine, M.D. Plasencia, X.Y. Liu, M. Krishnan, S. Naylor, H.R. Udseth, R.D. Smith, D.E. Clemmer, Toward plasma proteome profiling with ion mobility-mass spectrometry, Journal of Proteome Research 5 (11) (2006) 2977–2984.
[72] L.S. Fenn, M. Kliman, A. Mahsut, S.R. Zhao, J.A. McLean, Characterizing ion mobility-mass spectrometry conformation space for the analysis of complex biological samples, Analytical and Bioanalytical Chemistry 394 (1) (2009) 235–244.
[73] A.B. Kanu, P. Dwivedi, M. Tam, L. Matz, H.H. Hill, Ion mobility-mass spectrometry, Journal of Mass Spectrometry 43 (1) (2008) 1–22.
[74] S.J. Hyung, C.V. Robinson, B.T. Ruotolo, Gas-phase unfolding and disassembly reveals stability differences in ligand-bound multiprotein complexes, Chemistry & Biology 16 (4) (2009) 382–390.
[75] E.C. Chan, L.S. New, C.W. Yap, L.T. Goh, Pharmaceutical metabolite profiling using quadrupole/ion mobility spectrometry/time-of-flight mass spectrometry, Rapid Communications in Mass Spectrometry 23 (3) (2009) 384–394.
[76] A. Mie, A. Ray, B.O. Axelsson, M. Jornten-Karlsson, C.T. Reimann, Terbutaline enantiomer separation and quantification by complexation and field asymmetric ion mobility spectrometry-tandem mass spectrometry, Analytical Chemistry 80 (11) (2008) 4133–4140.
[77] P. Dwivedi, H.H. Hill Jr., A rapid analytical method for hair analysis using ambient pressure ion mobility mass spectrometry with electrospray ionization (ESI-IMMS), International Journal for Ion Mobility Spectrometry 11 (1–4) (2008) 61–69.
[78] G.A. Eiceman, D.A. Blyth, D.B. Shoff, A.P. Snyder, Screening of solid commercial pharmaceuticals using ion mobility spectrometry, Analytical Chemistry 62 (14) (1990) 1374–1379.
[79] H. Borsdorf, E.G. Nazarov, G.A. Eiceman, Atmospheric pressure chemical ionization studies of non-polar isomeric hydrocarbons using ion mobility spectrometry and mass spectrometry with different ionization techniques, Journal of American Society for Mass Spectrometry 13 (9) (2002) 1078–1087.
[80] Y.Y. Zhao, X. Liu, J.M. Boyd, F. Qin, J. Li, X.F. Li, Identification of N-nitrosamines in treated drinking water using nanoelectrospray ionization high-field asymmetric waveform ion mobility spectrometry with quadrupole time-of-flight mass spectrometry, Journal of Chromatographic Science 47 (1) (2009) 92–96.
[81] B.H. Clowers, W.E. Steiner, H.M. Dion, L.M. Matz, M. Tam, E.E. Tarver, H.H. Hill, Evaluation of sulfonylurea herbicides using high resolution electrospray ionization ion mobility quadrupole mass spectrometry, Field Analytical Chemistry and Technology 5 (6) (2001) 302–312.
[82] A. Mie, M. Sandulescu, L. Mathiasson, J. Emneus, T. Reimann Curt, Analysis of triazines and associated metabolites with electrospray ionization field-asymmetric ion mobility spectrometry/mass spectrometry, Analytical Sciences: The International Journal of the Japan Society for Analytical Chemistry 24 (8) (2008) 973–978.
[83] W.E. Steiner, S.J. Klopsch, W.A. English, B.H. Clowers, H.H. Hill, Detection of a chemical warfare agent simulant in various aerosol matrixes by ion mobility time-of-flight mass spectrometry, Analytical Chemistry 77 (15) (2005) 4792–4799.
[84] Hill, H.H. Jr., Dwivedi, P., Kanu, A.B., Reduction in false positive responses for explosives detection using ion mobility-mass spectrometry (IMMS). First Indo-US Workshop on Spectroscopy, vol. 14, Laser and Spectroscopy Society of India, B.H.U. Varanasi, India, 2006, pp. 92–103.
[85] M.J. Waltman, P. Dwivedi, H.H. Hill Jr., W.C. Blanchard, R.G. Ewing, Characterization of a distributed plasma ionization source (DPIS) for ion mobility spectrometry and mass spectrometry, Talanta 77 (1) (2008) 249–255.
[86] P. Dwivedi, P. Wu, S. Klopsch, G. Puzon, L. Xun, H. Hill, Metabolic profiling by ion mobility mass spectrometry (IMMS), Metabolomics (2007) (Published online: 11 December 2007).
[87] G.R. Asbury, H.H. Hill, Evaluation of ultrahigh resolution ion mobility spectrometry as an analytical separation device in chromatographic terms, Journal of Microcolumn Separations 12 (3) (2000) 172–178.
[88] C. Wu, W.F. Siems, G.R. Asbury, H.H. Hill Jr., Electrospray ionization high-resolution ion mobility spectrometry–mass spectrometry, Analytical Chemistry 70 (23) (1998) 10.
[89] W.E. Steiner, B.H. Clowers, K. Fuhrer, M. Gonin, L.M. Matz, W.F. Siems, A.J. Schultz, H.H. Hill, Electrospray ionization with ambient pressure ion mobility separation and mass analysis by orthogonal time-of-flight mass spectrometry, Rapid Communications in Mass Spectrometry 15 (23) (2001) 2221–2226.
[90] H.E. Revercomb, E.A. Mason, Theory of plasma chromatography/gaseous electrophoresis—a review, Analytical Chemistry 47 (7) (1975) 970.
[91] M. Sud, E. Fahy, D. Cotter, A. Brown, E.A. Dennis, C.K. Glass, A.H. Merrill Jr., R.C. Murphy, C.R. Raetz, D.W. Russell, S. Subramaniam, LMSD: LIPID MAPS structure database, Nucleic Acids Research 35 (Database issue) (2007) D527–D532.
[92] E. Fahy, S. Subramaniam, H.A. Brown, C.K. Glass, A.H. Merrill Jr., R.C. Murphy, C.R.H. Raetz, D.W. Russell, Y. Seyama, W. Shaw, T. Shimizu, F. Spener, G. van Meer, M.S. VanNieuwenhze, S.H. White, J.L. Witztum, E.A. Dennis, A comprehensive classification system for lipids, Journal of Lipid Research 46 (5) (2005) 839–862.
[93] C.A. Smith, G. O'Maille, E.J. Want, C. Qin, S.A. Trauger, T.R. Brandon, D.E. Custodio, R. Abagyan, G. Siuzdak, METLIN—a metabolite mass spectral database, Therapeutic Drug Monitoring 27 (6) (2005) 747–751.
[94] J. Kopka, N. Schauer, S. Krueger, C. Birkemeyer, B. Usadel, E. Bergmuller, P. Dormann, W. Weckwerth, Y. Gibon, M. Stitt, L. Willmitzer, A.R. Fernie, D. Steinhauser, GMD@CSB.DB: the Golm Metabolome Database, Bioinformatics 21 (8) (2005) 1635–1638.
[95] S.L. Koeniger, S.I. Merenbloom, S.J. Valentine, M.F. Jarrold, H.R. Udseth, R.D. Smith, D.E. Clemmer, An IMS–IMS analogue of MS–MS, Analytical Chemistry 78 (12) (2006) 4161–4174.
[96] S.I. Merenbloom, S.L. Koeniger, S.J. Valentine, M.D. Plasencia, D.E. Clemmer, IMS–IMS and IMS–IMS–IMS/MS for separating peptide and protein fragment ions, Analytical Chemistry 78 (8) (2006) 2802–2809.
[97] S.J. Valentine, R.T. Kurulugama, B.C. Bohrer, S.I. Merenbloom, R.A. Sowell, Y. Mechref, D.E. Clemmer, Developing IMS–IMS–MS for rapid characterization of abundant proteins in human plasma, International Journal of Mass Spectrometry 283 (1–3) (2009) 149–160.
[98] A.S. Woods, M. Ugarov, T. Egan, J. Koomen, K.J. Gillig, K. Fuhrer, M. Gonin, J.A. Schultz, Lipid/peptide/nucleotide separation with MALDI-ion mobility-TOF MS, Analytical Chemistry 76 (8) (2004) 2187–2195.
[99] B.H. Clowers, P. Dwivedi, W.E. Steiner, H.H. Hill Jr., B. Bendiak, Separation of sodiated isobaric disaccharides and trisaccharides using electrospray ionization-atmospheric pressure ion mobility-time of flight mass spectrometry, Journal of American Society of Mass Spectrometry 16 (5) (2005) 660–669.
[100] P. Dwivedi, B. Bendiak, B.H. Clowers, H.H. Hill Jr., Rapid resolution of carbohydrate isomers by electrospray ionization ambient pressure ion mobility spectrometry-time-of-flight mass spectrometry (ESI-APIMS-TOFMS), Journal of the American Society for Mass Spectrometry 18 (7) (2007) 1163–1175.
[101] P. Britz-McKibbin, S. Terabe, On-line preconcentration strategies for trace analysis of metabolites by capillary electrophoresis, Journal of Chromatography A 1000 (1–2) (2003) 917–934.
[102] C. Lidebjer, P. Leanderson, J. Ernerudh, L. Jonasson, Low plasma levels of oxygenated carotenoids in patients with coronary artery disease, Nutrition, Metabolism, and Cardiovascular Diseases 17 (6) (2007) 448–456.
[103] Y. Kita, T. Takahashi, N. Uozumi, L. Nallan, M.H. Gelb, T. Shimizu, Pathway-oriented profiling of lipid mediators in macrophages, Biochemical and Biophysical Research Communications 330 (3) (2005) 898–906.
[104] C.N. Serhan, Mediator lipidomics, Prostaglandins & Other Lipid Mediators 77 (1–4) (2005) 4–14.
[105] S.N. Jackson, H.Y.J. Wang, A.S. Woods, Direct tissue analysis of phospholipids in rat brain using MALDI-TOFMS and MALDI-ion mobility-TOFMS, Journal of the American Society for Mass Spectrometry 16 (2) (2005) 133–138.
[106] B.T. Ruotolo, K.J. Gillig, E.G. Stone, D.H. Russell, Peak capacity of ion mobility mass spectrometry: separation of peptides in helium buffer gas, Journal of Chromatography B Analytical Technologies in Biomedical and Life Sciences 782 (1–2) (2002) 385–392.

[107] B.T. Ruotolo, G.F. Verbeck, L.M. Thomson, A.S. Woods, K.J. Gillig, D.H. Russell, Distinguishing between phosphorylated and nonphosphorylated peptides with ion mobility-mass spectrometry, Journal of Proteome Research 1 (4) (2002) 303–306.
[108] M. Morris, S.M. Watkins, Focused metabolomic profiling in the drug development process: advances from lipid profiling, Current Opinion in Chemical Biology 9 (4) (2005) 407–412.
[109] B.T. Ruotolo, K.J. Gillig, E.G. Stone, D.H. Russell, Peak capacity of ion mobility mass spectrometry: separation of peptides in helium buffer gas, Journal of Chromatography B, Analytical Technologies in the Biomedical and Life Sciences 782 (1) (2003) 8.
[110] J.L. Frahm, B.E. Howard, S. Heber, D.C. Muddiman, Accessible proteomics space and its implications for peak capacity for zero-, one- and two-dimensional separations coupled with FT-ICR and TOF mass spectrometry, Journal of Mass Spectrometry 41 (3) (2006) 281–288.
[111] D.J. Rose, G.J. Opiteck, Two-dimensional gel electrophoresis/liquid chromatography for the micropreparative isolation of proteins, Analytical Chemistry 66 (15) (1994) 2529–2536.
[112] J.A. McLean, B.T. Ruotolo, K.J. Gillig, D.H. Russell, Ion mobility-mass spectrometry: a new paradigm for proteomics, International Journal of Mass Spectrometry 240 (3) (2005) 301–315.
[113] X.Y. Liu, S.J. Valentine, M.D. Plasencia, S. Trimpin, S. Naylor, D.E. Clemmer, Mapping the human plasma proteome by SCX-LC–IMS-MS, Journal of the American Society for Mass Spectrometry 18 (7) (2007) 1249–1264.
[114] S.I. Merenbloom, B.C. Bohrer, S.L. Koeniger, D.E. Clemmer, Assessing the peak capacity of IMS-IMS separations of tryptic peptide ions in He at 300 K, Analytical Chemistry 79 (2) (2007) 515–522.
[115] E.J. Want, G. O'Maille, C.A. Smith, T.R. Brandon, W. Uritboonthai, C. Qin, S.A. Trauger, G. Siuzdak, Solvent-dependent metabolite distribution. Clustering, and protein extraction for serum profiling with mass spectrometry, Analytical Chemistry 78 (3) (2006) 743–752.
[116] S.M. Roy, M. Anderle, H. Lin, C.H. Becker, Differential expression profiling of serum proteins and metabolites for biomarker discovery, International Journal of Mass Spectrometry 238 (2) (2004) 163–171.
[117] A. Nordstrom, G. O'Maille, C. Qin, G. Siuzdak, Nonlinear data alignment for UPLC–MS and HPLC–MS based metabolomics: quantitative analysis of endogenous and exogenous metabolites in human serum, Analytical Chemistry 78 (10) (2006) 3289–3295.